ACS Chemical Neuroscience

Research Article

Cite This: ACS Chem. Neurosci. 2017, 8, 2512-2521

pubs.acs.org/chemneuro

Comparison of Spreading Depolarizations in the Motor Cortex and Nucleus Accumbens: Similar Patterns of Oxygen Responses and the Role of Dopamine

Caddy N. Hobbs,[†] Gordon Holzberg,[†] Akira S. Min,[†] and R. Mark Wightman*[,†,‡]

[†]Department of Chemistry, University of North Carolina at Chapel Hill, Chapel Hill, North Carolina 27599, United States

[‡]Neuroscience Center, University of North Carolina at Chapel Hill, Chapel Hill, North Carolina 27599, United States

ABSTRACT: Spreading depolarizations (SD) are pathophysiological phenomena that spontaneously arise in traumatized neural tissue and can promote cellular death. Most investigations of SD are performed in the cortex, a brain region that is susceptible to these depolarizing waves and accessible via a variety of monitoring techniques. Here, we describe SD responses in the cortex and the deep brain region of the nucleus accumbens (NAc) of the anesthetized rat with a minimally invasive, implantable sensor. With high temporal resolution, we characterize the time course of oxygen responses to SD in relation to the electrophysiological depolarization signal. The predominant oxygen pattern consists of four phases: (1) a small initial decrease, (2) a large increase during the SD, (3) a delayed increase, and (4) a persistent decrease from baseline after the SD. Oxygen decreases during SD were also recorded. The latter response occurred more often in the NAc than the cortex (56% vs 20% of locations, respectively), which correlates to denser cortical vascularization. We also find that SDs travel more quickly in the cortex than NAc, likely affected by regional differences in cell type populations. Finally, we investigate the previously uncharacterized effects of dopamine release during SD in the NAc with dopamine receptor blockade. Our results support an inhibitory role of the D2 receptor on SD. As such, the data presented here expands the current understanding of within- and between-region variance in responses to SD.

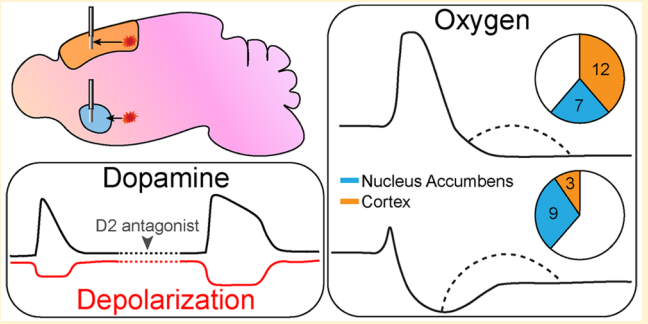

KEYWORDS: *Spreading depolarization, dopamine, oxygen, DC electrophysiology, biosensors, brain trauma*

INTRODUCTION

Spreading depolarizations (SD) are pathological events characterized by one of the largest changes in electrophysiological activity and extracellular ion concentrations that occur in neural tissue.[1,2] Extracellular potassium increases from ~3.5 to over 30 mM. Also, sodium, calcium, and chloride ions enter the cells, accompanied by water.[3,4] These ionic imbalances lead to the release of neurotransmitters such as glutamate, dopamine, and adenosine into the extracellular space.[5−9] The drastic changes in the concentrations of intra- and extracellular species during SD inflict a considerable metabolic challenge on the tissue.

The typical hemodynamic response to SD in otherwise healthy tissue is an increase in cerebral blood flow followed by a long-lasting decrease below baseline.[10] The rise in blood flow delivers oxygen and glucose, which provide energy to the metabolically challenged tissue to restore its ion gradients.[10−13] However, a deficit in oxygen and glucose can promote cell death by prolonging the duration of ionic disruption and cellular swelling.[14−18] Oxygen concentration changes represent the balance between blood flow delivery and metabolic consumption; thus, they serve as a valuable indicator of the metabolic state of the tissue. However, conflicting reports of oxygen concentration responses to SD arise due to differences in experimental protocol such as anesthesia, surgical procedures, and animal models.[12,19−23] Furthermore, differences in neurovascular microarchitecture can affect the oxygen concentrations recorded during SD.[23]

Here, we characterize interlocation variability in oxygen responses to SDs in the traditionally studied cortex and a deeper brain region with dopaminergic innervation, the nucleus accumbens (NAc), of the urethane-anesthetized rat. We employ a recently described, multimodal sensor with subsecond resolution that is capable of simultaneously recording oxygen, electroactive neurotransmitters, and DC potential electrophysiology.[24] With the 5 μm diameter and μm-spatial resolution of our sensor, we minimize the confounding effects of tissue damage and are able to detect variance in oxygen responses in normally perfused tissue due to spatial heterogeneity. As distinct brain regions are differentially susceptible to SD[2,25] and have variable vascularization[26] and cell-type populations,[27,28] we hypothesize that SD may promote different effects in these two

Received: July 12, 2017
Accepted: August 18, 2017
Published: August 18, 2017

DOI: 10.1021/acschemneuro.7b00266
ACS Chem. Neurosci. 2017, 8, 2512−2521

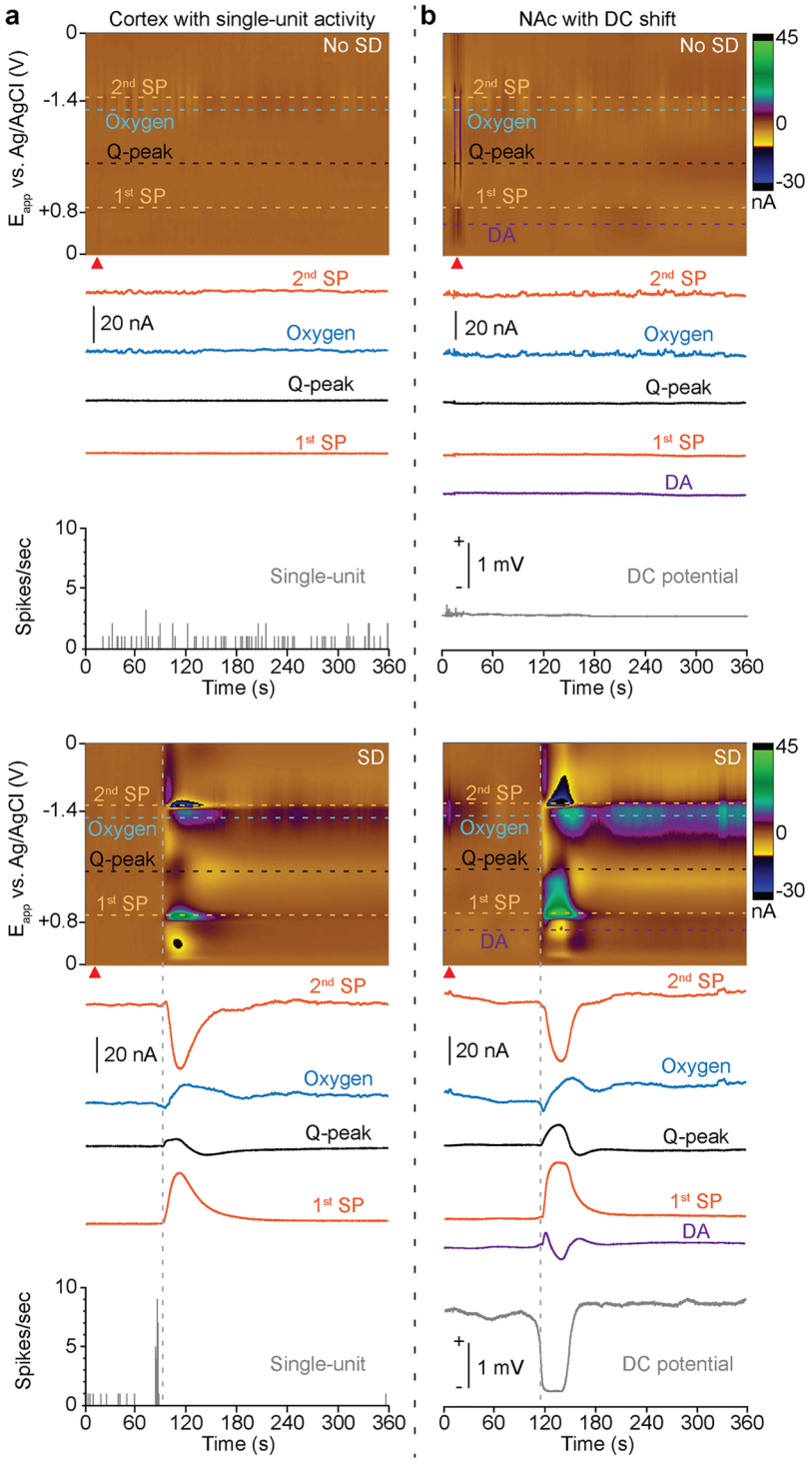

Figure 1. Simultaneous electrophysiological and voltammetric recordings. Voltammetric data displayed as color plots with corresponding current traces and electrophysiological data shown below. Red triangles indicate time of stimulus. Vertical gray dashed line indicates onset of spreading depolarization (SD) as determined from voltammetric signals. Horizontal dashed lines in the color plots indicate the potential location of currents arising from capacitive artifacts at the switching potentials (SP, orange), surface-bound quinone moieties (Q-peak, black), oxygen reduction (blue), and dopamine oxidation (DA, purple). Corresponding current traces shown below the color plots. Top panel, stimulation failed to produce SD. Lower panel, successfully induced SD. (a) Cortex location with single-unit activity. (b) NAc location with DC electrophysiological recordings.

brain regions. Finally, we investigate the modulatory role of dopamine on SD in the NAc with pharmacological manipulation.

RESULTS

Simultaneous Voltammetric and Electrophysiology Recordings. We previously characterized an implantable, multimodal sensor for real-time voltammetric detection of oxygen and electroactive neurotransmitters with simultaneous electrophysiological recordings.[24] The small dimensions (5 μm diameter) of the sensor yield spatially and temporally resolved chemical information and allow for minimally invasive recordings in deep brain tissue. In the traditionally studied cortex and a

DOI: 10.1021/acschemneuro.7b00266
ACS Chem. Neurosci. 2017, 8, 2512−2521

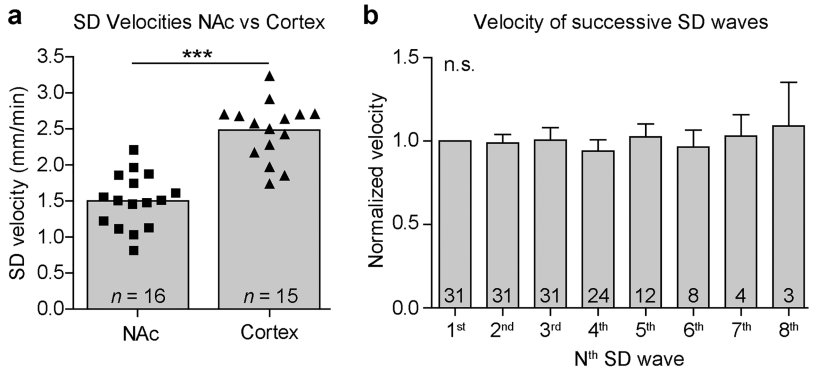

Figure 2. Spreading depolarization (SD) velocity analysis. (a) Average velocities for SD waves in the nucleus accumbens (NAc) and cortex. Columns indicate the means of the two sample sets. Mean velocities of each recording site are plotted; NAc, squares; cortex, triangles. The velocities are significantly different between the two brain regions ($p < 0.001$, two-tailed t test). (b) Velocity changes for successive SD waves within location. The magnitude of the velocities in a given recording location were normalized to the first response within that location. Numbers of locations included for each successive SD event are indicated along the x-axis. Bars indicate ± SEM.

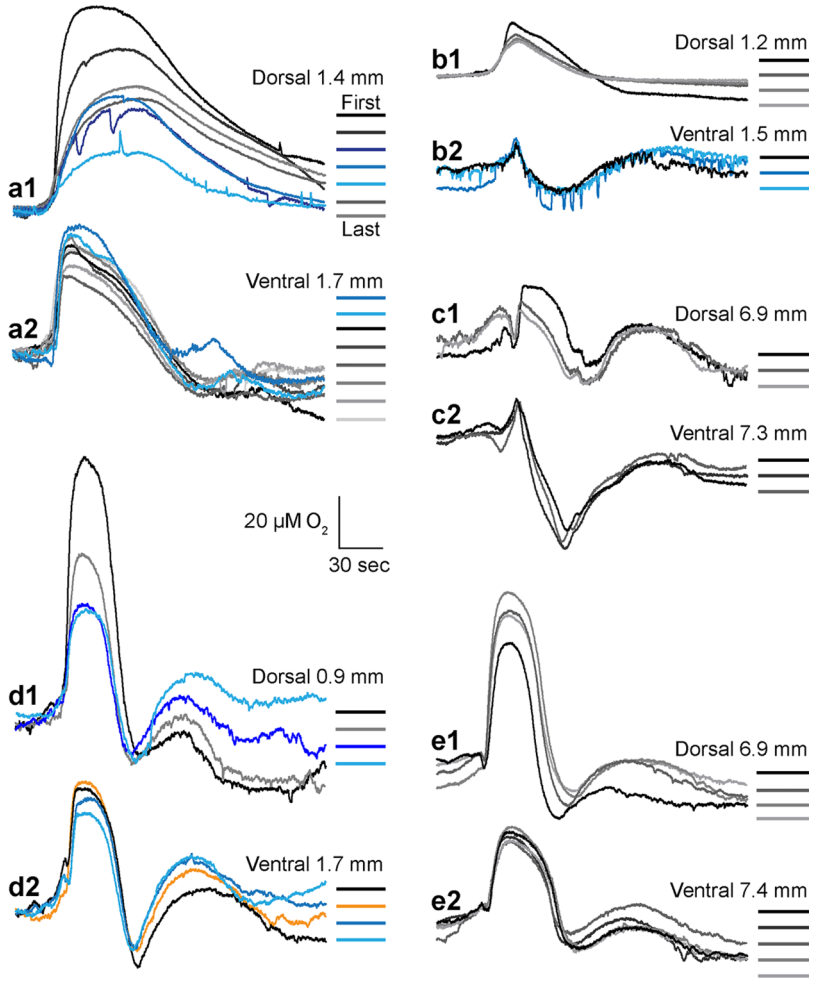

Figure 3. Oxygen traces during successive SD waves from five animals with two recording locations each. Color keys to the right define the order of responses to successive SD waves, first to last, top to bottom. Different colors (e.g., blue scale vs gray scale) signify a different stimulus location. Dorsal-ventral depth of recording location specified above color key. Traces within a location are temporally aligned to the onset of depolarization. (a) Two cortical locations, separated by 0.3 mm. (b) Two cortical locations in a different subject, separated by 0.3 mm. (c) Two NAc locations, separated by 0.4 mm. (d) Two cortical locations, separated by 0.8 mm. (e) Two NAc locations, separated by 0.5 mm.

deeper brain region, the NAc, we make comparative investigations of electrophysiological and chemical changes during SD. Both responses are recorded at a carbon-fiber working electrode ∼2−4 min after delivery of a stimulus at a defined location 3−5 mm away. The chemical signals are comprised of large current deviations in successive cyclic voltammograms of the color plot (Figure 1). Traces from the color plot are obtained at the potentials for oxidation of dopamine (+0.65 V on the initial

DOI: 10.1021/acschemneuro.7b00266
ACS Chem. Neurosci. 2017, 8, 2512−2521

positive voltage excursion) and reduction of oxygen (−1.33 V on the negative voltage excursion). Also, ion concentration changes occurring during SD produce large currents that manifest after the switching potentials (SP) of the waveform (+0.8 and −1.4 V) and at −0.1 V on the negative scan (Q-peak) (Figure 1).[24] Concomitantly recorded electrophysiological changes confirm the occurrence of a SD for the lower two traces (Figure 1). These changes appear as a burst of neuron firing followed by silence during single-unit recording or as a large, negative deflection of the extracellular DC potential which slightly precedes (5−10 s) the onset of the voltammetric signal (Figure 1). SD was not achieved in the upper two traces as indicated by the electrophysiological measures, and only minor chemical changes were recorded in these locations.

SD Velocity and Induction. The distance between the stereotaxic positions of the stimulus and recording locations were used to calculate the SD velocity (eq 1). SD waves propagate more quickly through cortical tissue than through the ventral striatum (cortex: 2.5 ± 0.1 mm/min, n = 15 locations versus NAc: 1.5 ± 0.1 mm/min, n = 16 locations; Student's t test, p < 0.0001; Figure 2a). The SD velocity did not change significantly over successive pricks in a single location (one-way ANOVA, n = 31, F = 0.2087, p = 0.9830; Figure 2b). Additionally, SDs were more likely to be elicited and propagate to our sensor in the cortical experiments as compared to those in the NAc. If two successive pinpricks failed to trigger SD, a KCl microinfusion was delivered instead (first 250 mM, then 1 M). KCl microinfusions were required in 63% of NAc locations, as opposed to only 13% of cortex locations. Student's t tests were performed to evaluate for any systematic differences in the calculated SD velocity caused by the two different methods of stimulation. In the cortex, the average SD velocities for locations where pin pricks were used (n = 13) were not significantly different from the average velocities for locations where KCl microinfusions were delivered (n = 2). Locations in the NAc where KCl microinfusions (n = 10) were used had significantly higher calculated average SD velocities as compared to locations where pin pricks (n = 6) were employed (1.7 ± 0.1 vs 1.2 ± 0.1 mm/min, Student's t test, p = 0.0295). This difference may be due to the KCl droplet radius shortening the distance traveled by the SD wave or the microinfusion method more rapidly initiating the SD. However, it does not affect the finding that SDs traveled more quickly in the cortex than the NAc.

Successive Oxygen Responses within a Recording Location. We found that oxygen responses differed between recording sites, but were similar for successive depolarizations within a single location. The reproducibility across successive responses was evaluated by normalizing the oxygen maxima during the SDs to the first response's amplitude within a location. The amplitude of the responses did not change significantly over successive SDs (one-way ANOVA, n = 31, F = 0.70667, p = 0.6663). In five subjects, oxygen responses to SD waves were recorded in two sequential sites of the same brain region, separated by at least 0.3 mm on the DV axis (Figure 3). The oxygen traces in Figure 3a−c had some variance in magnitude, duration, and/or profile between the two recording sites. In two subjects, the oxygen recordings for locations separated by 0.8 and 0.5 mm were more similar (Figure 3d,e, respectively).

The oxygen change profiles across successive SD waves were similar within a given location. However, a small subset of recording locations (n = 2/31, or 6.5%) depicted variance in responses at the same recording position for different stimulation sites (Figure 4). In one recording location, the first stimulation

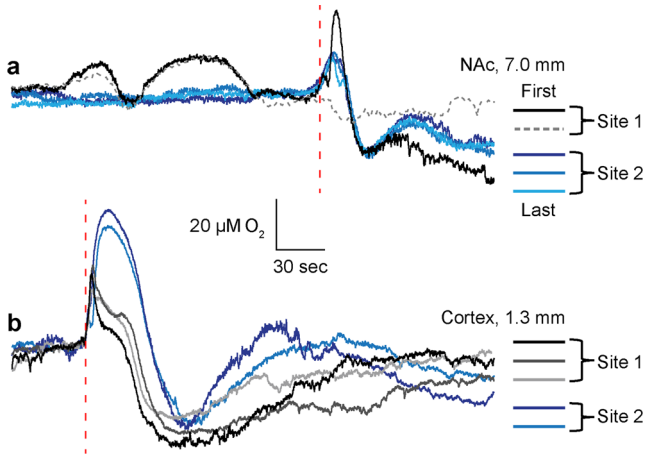

Figure 4. Oxygen traces during successive SD waves in recording locations where the response varied based on stimulation location. Color keys to the right define the order of responses to successive SD waves, first to last, top to bottom. Different colors (e.g., blue scale vs gray scale) signify a different stimulus location. Traces for each recording location are temporally aligned to the SD onset (vertical, red dashed line). (a) Pinprick stimuli at Site 1 (gray scale; −0.8 mm AP, + 3.2 mm ML) elicited a two-peaked oxygen increase that arrived in the recording location before the wave of SD (black trace) or without a following SD wave (gray dashed trace). Pinprick stimuli at Site 2 (blue scale; −0.8 AP mm, + 0.8 mm ML) did not elicit two-peak oxygen increase before SD. (b) Pinprick stimuli delivered in two different locations elicited oxygen responses with varied profiles (Site 1, gray scale, −0.8 AP mm, + 0.8 mm ML; Site 2, blue scale, −0.8 mm AP, + 3.2 mm ML).

elicited a two-peaked oxygen increase that began before the SD signal arrived, followed by oxygen changes with the SD (Figure 4a, Site 1, black trace). In contrast, the second stimulation at the same site evoked the pre-SD oxygen response but did not evoke SD or its accompanying oxygen changes (Figure 4a, Site 1, gray dashed trace). At the same recording position, stimulation at the second location did not evoke pre-SD oxygen increases, but did yield the oxygen changes associated with the SD (Site 2, blue traces, Figure 4a). Another location also showed differences in the oxygen responses based on the location at which the stimulation was delivered (Figure 4b). Both responses were biphasic increases, but the magnitudes and profiles differed.

Four Types of Oxygen Changes Accompanying SD. In the cortex and NAc of the urethane-anesthetized rat, oxygen responses were categorized into four patterns as a function of their changes relative to the SD (n = 31 locations). The majority of locations (n = 19, or 61%) had an oxygen increase during the SD (Figure 5a,b). These were divided into two groups—those with another oxygen increase after the SD (11 locations, termed biphasic) and those without (8 locations, termed monophasic). The remainder (12 locations) showed an oxygen decrease during the SD (Figure 5c,d). Again, these were subdivided into those that showed an oxygen increase after SD (10 locations, termed decrease/increase) and those that did not (2 locations, termed decrease). The cortex had a higher percentage of oxygen "increase" responses (80%) as compared to the NAc (44%).

Four phases of the oxygen response were labeled with roman numerals in Figure 5: (I) a small initial decrease, (II) an increase occurring with the SD, (III) a delayed increase after the SD, and (IV) a persistent decrease from baseline after the SD. This nomenclature corresponds to the four components of blood flow changes occurring with SD in normally perfused tissues, examined further in the discussion.[10,29] The average peak and

DOI: 10.1021/acschemneuro.7b00266
ACS Chem. Neurosci. 2017, 8, 2512−2521

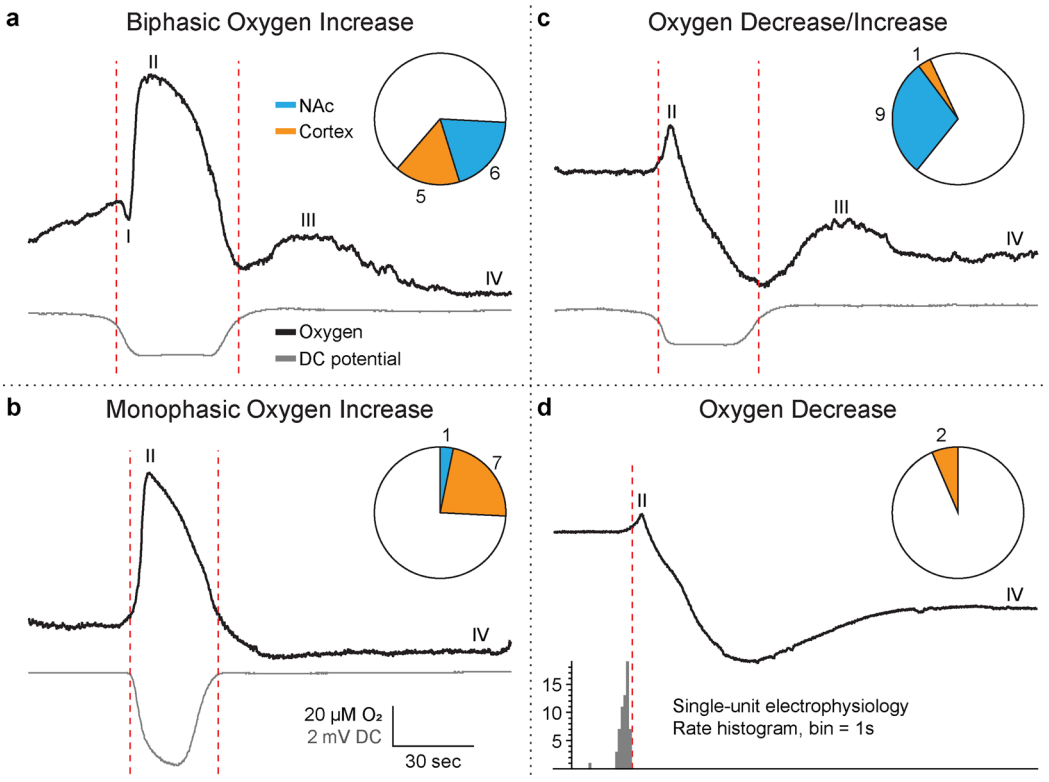

Figure 5. Representative oxygen traces and electrophysiological recordings from four different locations depicting the types of oxygen responses recorded during SD. Electrophysiological recordings (gray) are displayed below the oxygen traces (black). Red vertical dashed lines indicate temporal boundaries of electrophysiological depolarization signals. Roman numeral I, initial decrease in oxygen; II, main oxygen increase peak; III, delayed increase in oxygen; IV, long-lasting decrease below baseline. Pie charts in the upper right-hand corner of the quadrants give the number of locations of each response type (NAc locations in blue, cortex locations in orange). (a) Biphasic oxygen increase with DC potential. (b) Monophasic oxygen increase with DC potential. (c) Oxygen decrease during SD and a following increase with DC potential. (d) Oxygen decrease during SD with single-unit activity. Because of their rarity, no oxygen responses of this type were obtained with DC electrophysiological recordings.

Table 1. Magnitude of Changes for the Four Types of Oxygen Responses during SD[a]

	increase during SD (μM)	decrease during SD (μM)	Phase III (μM)	Phase IV (μM)	duration of Phase II (s)	duration of Phase III (s)
biphasic increase (n = 11)	47 ± 9		7 ± 4	−8 ± 4	48 ± 4	89 ± 9
monophasic increase (n = 8)	38 ± 7			−11 ± 2	112 ± 24	
decrease/increase (n = 10)		−56 ± 10	−14 ± 3	−23 ± 3	17 ± 3	51 ± 5
decrease (n = 2)		−25 ± 12		−8 ± 3	20 ± 2	

[a]Values presented as average ± SEM.

trough oxygen concentrations and durations of the peaks are given in Table 1 (there were no differences between brain regions). The initial dip in oxygen concentration, Phase I, was apparent in 52% of all locations (n = 10 NAc, n = 6 cortex). However, it was not always reproducibly present: Six of those locations had one or more oxygen responses to SD waves that lacked Phase I. This initial decrease was relatively small (2.4 ± 0.2 μM) compared to the other oxygen changes (compare with values in Table 1).

Dopamine Release and Pharmacological Manipulation during SD in the NAc. Recordings of SDs in the NAc were all accompanied by a large release (13.0 ± 1.8 μM, n = 10 subjects, predrug concentrations) of dopamine that was highly reproducible for successive SD waves within a recording location (a representative color plot and cyclic voltammogram are shown in Figure 6a). To pharmacologically investigate the possible effects of dopamine on SD, we recorded two SDs and then administered raclopride or SCH 23390 (selective D2- and D1-receptor antagonists, respectively) by i.p. injection (n = 5 subjects per drug). At 45 min later, 3−4 succeeding SD episodes were evoked. Pre- and postdrug administration averaged values were analyzed by paired, two-tailed t tests (Figure 6b,c).

The dopamine peak decay time and DC shift magnitude both significantly increased with D2-receptor antagonism (respectively, 13.8 ± 2.8 to 29.1 ± 5.7 s, n = 5, p = 0.035; 2.4 ± 0.2 to 4.3 ± 0.6 mV, n = 5, p = 0.032; Figure 6). While SD velocity increased, it did not reach significance (1.2 ± 0.1 to 1.7 ± 0.3 mm/min, n = 5, p = 0.057; Figure 6). Also, the DC shift half-width increased with raclopride administration, but not significantly (37.2 ± 10.0 to 50.3 ± 6.8 s, n = 5, p = 0.052; Figure 6). D1-receptor antagonism attenuated the dopamine peak magnitude (14.9 ± 2.3 to 10.6 ± 1.7 μM, p = 0.0078, n = 5; Figure 6), but did not significantly affect the SD velocity, the DC magnitude, or the DC duration.

Similar experiments were conducted in the cortex. As expected, no catecholamine signals were observed in the cortex during SD (Figure 7a). The cyclic voltammogram does not resemble that for dopamine, and the remaining current is from

DOI: 10.1021/acschemneuro.7b00266
ACS Chem. Neurosci. 2017, 8, 2512−2521

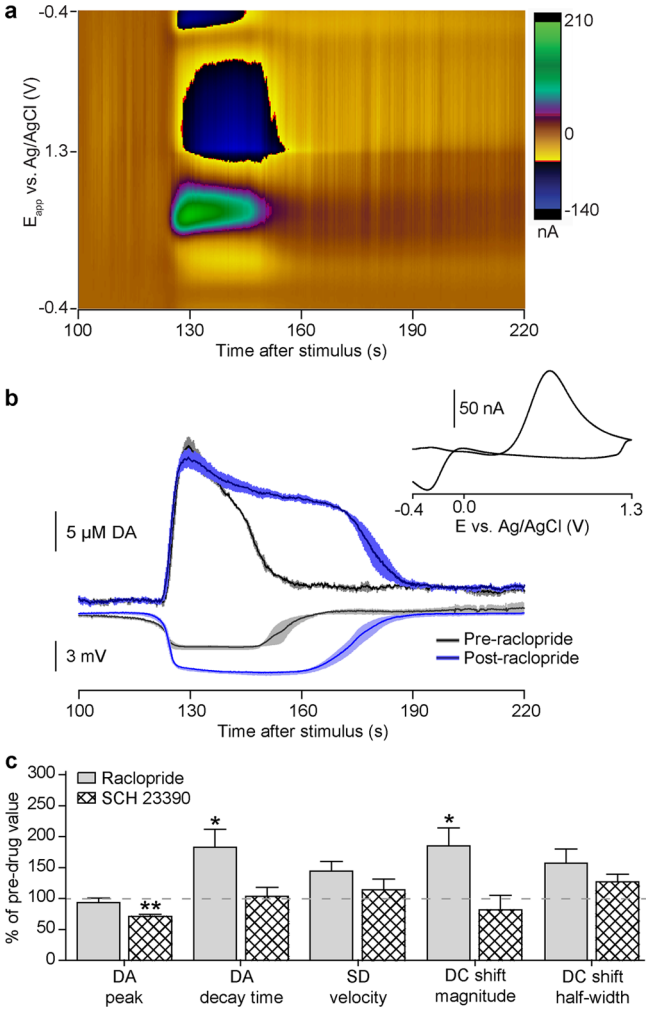

Figure 6. Effect of dopamine (DA) receptor antagonism on DA release, SD velocity, and DC potential shift in the NAc. (a) Representative color plot of SD event with the convolution-based method waveform. (b) Average ± SEM DA release and DC electrophysiology traces during SD waves in a single location, before (black) and after (blue) administration of raclopride. Inset: cyclic voltammogram from (a) at 130 s that is identical to that for dopamine. (c) Analysis of changes in DA peak concentration, DA decay time ($t_{1/2}$), SD velocity, DC shift magnitude, and DC shift half-width (a measure of duration) after administration of raclopride or SCH 23390 ($n = 5$ animals per drug). Significance between pre- and postdrug values was analyzed by paired, two-tailed t tests: $*p < 0.05$, $**p < 0.01$.

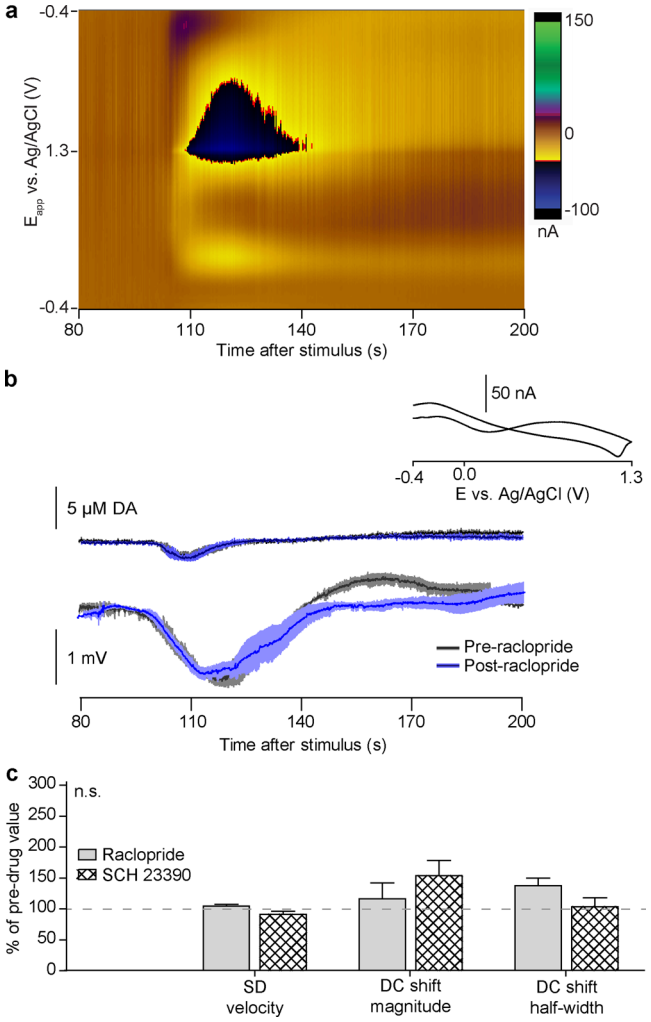

Figure 7. Effect of dopamine (DA) receptor antagonism on SD velocity and DC potential shift in the cortex. (a) Representative color plot of SD event in the cortex with the convolution-based method waveform. (b) Average ± SEM trace at the oxidation potential for DA and DC electrophysiology traces during SD waves in a single location, before (black) and after (blue) administration of raclopride. Inset: cyclic voltammogram from (a) at 105 s. (c) Analysis of changes in SD velocity, DC shift magnitude, and DC shift half-width (a measure of duration) after administration of raclopride or SCH 23390 ($n = 4$ animals per drug). There was no significance between pre- and postdrug values, analyzed by paired, two-tailed t tests.

uncorrected interferences following the convolution-based subtraction method (Figure 7b).[30] Furthermore, no significant changes were observed in the DC potential following dopamine antagonists (Figure 7b,c).

DISCUSSION

The results presented here clearly support the utility of the multimodal sensor that we developed to investigate the physiological and chemical changes occurring during SD in cortical and deeper brain regions. Two different measures of physiology were used to demonstrate that the applied stimuli evoked SD. The DC potential was considered more useful because of the paucity of unit firing in the anesthetized preparation and the quantifiable nature of the DC signal. The simultaneous chemical measures showed that the concentration changes of oxygen followed similar patterns in the two investigated brain regions. Recordings of dopamine in the NAc showed that its supraphysiological release occurs with the SD and that it exerts inhibitory effects on SD through interactions with D2 receptors.

SD Propagates More Quickly in the Cortex than in the Ventral Striatum. SD velocity was faster in the cortex than in the ventral striatum (Figure 2a), and SDs were more likely to be initiated in the cortex as compared to the NAc. Differences in susceptibility to SD for different brain structures have been well documented,[2,25] and SD velocity has been correlated to a region's susceptibility to SD.[31] Variation in inherent excitability of neurons is one cause of contrasting vulnerability.[32] Brisson and Andrew[33] proposed another: differing efficacy of Na^+-K^+-ATPase pumps between neuronal populations. Additionally, astrocytes impede SD propagation by clearing the extracellular space of potassium ions and glutamate.[6,34] Accordingly, regions with

DOI: 10.1021/acschemneuro.7b00266
ACS Chem. Neurosci. 2017, 8, 2512−2521

higher densities of astrocytes have slower velocity SD waves.[35] The higher density of astrocytes in the NAc as compared the cortex[36] likely is partially responsible for the decreased susceptibility and propagation speed of SD found in that region.

Oxygen Responses Are Highly Similar within Locations and Variable between Locations. Oxygen concentration serves as a marker of the balance between blood flow and metabolism, which dictates the outcome of tissue health. However, the use of different anesthetics[37,38] and surgical procedures that alter physiological responsivity[39,40] have yielded inconsistent reports of blood flow and oxygen concentration changes[12,19,20,22] during SD waves. To obviate these complications, we used a minimally invasive sensor to characterize oxygen changes in multiple locations in both the NAc and cortex of the urethane-anesthetized rat.

Oxygen responses accompanying successive SD events were reproducible (Figure 3), as previously reported for SDs in otherwise healthy tissue.[12,19,41] The magnitudes of these responses (Table 1) are similar to reported basal concentrations of oxygen,[42] indicating that oxygen concentrations could be approximately doubled or decreased to near zero during SD. These massive alterations in oxygen content emphasize the supraphysiological nature of SD.

Because of the high temporal and spatial resolution of FSCV at microelectrodes, our data further the current understanding of SD. First, our findings confirm previous reports of spatial heterogeneity of oxygen availability, as indirectly measured by NADH fluorescence.[23] In three subjects with two recording locations within the same brain region, different oxygen profiles were recorded in sites separated by 300−400 μm (Figure 3a−c); but, similar oxygen responses were recorded in the pairs of sites from two subjects (Figure 3d,e). Second, our oxygen recordings expand upon the finding of Brennan and colleagues[43] that dilatation of vessels in the cortex both preceded the SD and occurred in areas that the SD never reached—through a phenomenon known as distinct vascular conduction. This phenomenon would yield recordings like those in Figure 4a (a NAc location), where there is a reproducible change in oxygen both occurring ahead of the SD and in the absence of a SD. Furthermore, different stimulation locations yielded dissimilar oxygen changes for one recording site (Figure 4b). Though we cannot differentiate between the effects of different "upstream" neural networks or vasculature affecting the oxygen responses through cellular metabolism or vascular capacity, these data provide new evidence for heterogeneous responses to SD.

SD Waves Evoke Oxygen Increases and Decreases in Both the Cortex and NAc. The four-component scheme of blood flow changes during SD recently reviewed by Ayata and Lauritzen is well established,[10] and we used it to evaluate the different stages of our recorded oxygen traces (Figure 5): Phase I, initial dip; Phase II, main increase; Phase III, delayed increase; Phase IV, fall below baseline. Further, we designated four patterns of oxygen changes based on the presence and magnitude of these Phases: biphasic increase, monophasic increase, decrease/increase, and decrease (Figure 5). In the following discussion of the four profiles of recorded oxygen changes, we consider both underlying blood flow and metabolism alterations.

A period of hyperperfusion is reported to occur in normally perfused tissues during SD,[10−13,44] and would cause an increase in oxygen (Phase II). We hypothesize that the locations with oxygen decreases during SD received oxygen-depleted blood[23] or had metabolic consumption that surpassed the increase in blood flow. The decrease in oxygen began simultaneously with the maximal depolarization signal, or the voltage plateau of the electrophysiological DC shift (Figure 5c). This coincides with the greatest disruption in ion gradients, when ion pumps must consume energy in order to restore the membrane potential. Interestingly, 56% of NAc locations were designated as decreases, whereas only 20% of cortical locations were (Figure 5). This difference correlates with the generally larger diameter vessels and denser capillary vascularization in the cortex compared to deeper brain regions.[45,46] Additionally, most (94%) NAc locations exhibited a second oxygen increase (Phase III), as opposed to 40% of cortical locations (Figure 5). Traces with Phase III are consistent with recordings demonstrating a delayed blood flow increase.[10,29,44] The longer duration of the oxygen increase for the monophasic increase response type suggests that Phase II and III may have presented as one peak for these locations (Table 1).

High Levels of Extracellular Dopamine during SD Lowers Threshold of Propagation. SD initiation and propagation depend on critical thresholds being reached[2] for extracellular potassium, glutamate, and other species involved in neuronal excitability and depolarization.[3,4,47−50] These critical thresholds may be affected by dopamine, which exerts inhibitory and excitatory effects through the D2 and D1 receptors, respectively.[27,51,52] Early investigations in the striatum employed chronoamperometry to provide evidence suggesting that dopamine release was evoked during SD.[7,53] Recently this assignment was verified using a very fast microdialysis technique.[9] The modified FSCV procedure used in this work allows subsecond dopamine detection with simultaneous electrophysiology recording.[24] Here, we provide insight on dopamine's role in SD by investigating the effect of dopamine receptor blockade on dopamine release and uptake dynamics as well as DC potential changes.

D1-receptor antagonism decreased the peak dopamine concentration (Figure 6), consistent with blocking the excitatory effects of D1 activation. This indicates that under certain circumstances it is possible to modulate the amount of neurotransmitter released during SD. D2-receptor antagonism increased the dopamine peak decay time (Figure 6), in agreement with the effect of blocking the receptor's inhibitory autoreceptor function.[52] Also following D2-receptor antagonism, the amplitude of the DC shift increased. We hypothesize that blocking D2 receptors increases the amount of inward cation flux during depolarization.[54] Alternatively, D2-receptor blockade may reveal the dual effects of D1-receptor activation, increasing hyperpolarizing potassium currents, but also increasing neuronal excitability once the neuron is depolarized sufficiently.[51,54] Thus, the resting membrane potentials of neurons would be held at a more negative potential with respect to the extracellular space; then, during SD, they would undergo a larger change in membrane potential, or depolarization, producing a larger magnitude DC shift. The increase in SD velocity under D2-receptor antagonism (not significant, $p = 0.057$; Figure 6) also supports an inhibitory effect through D2-receptor activation, which may be another contributing factor to the slower SD velocity recorded in the NAc (Figure 2a).

■ CONCLUSIONS

Here, we investigated chemical and physiological changes during SD in normally perfused brain tissue. The high spatial resolution of FSCV allowed characterization of various oxygen responses to SD and they corresponded to well-documented blood flow changes. We identified four main response types for locations in

DOI: 10.1021/acschemneuro.7b00266
ACS Chem. Neurosci. 2017, 8, 2512−2521

both the cortex and NAc, defined by an increase or decrease in oxygen during the SD and by the presence or absence of a delayed oxygen increase peak following the SD. Interestingly, responses in the cortex were predominantly increases; whereas oxygen changes in the NAc were more evenly divided between increases and decreases. These findings may indicate that the vasculature of the deep brain is less able to deliver adequate oxygen to tissue during SD; however, higher metabolic demand in the NAc cannot be discounted as another possible explanation.

With the chemical specificity and temporal resolution afforded FSCV, we were able to probe the effects of dopamine during SD in the deep brain. A supraphysiological release of dopamine accompanied the depolarization signal for all recordings in NAc locations. Blockade of D1-receptors reduced the maximum amount of dopamine released during SD, establishing that attenuation of neurotransmitter release is possible during these "all-or-nothing" events. Additionally, D2-receptor antagonism increased the dopamine decay time and DC shift magnitude, which supports an inhibitory effect of this dopamine receptor on SD.

METHODS

Chemicals. All chemicals were obtained from Sigma-Aldrich (St. Louis, MO), unless otherwise specified.

Animal Care and Stereotactic Surgery. All techniques were carried out in accordance with the Institutional Animal Care and Use Committee of the University of North Carolina at Chapel Hill. Experiments were performed in male Sprague−Dawley rats (350−550 g) anesthetized by a 1.5 g/kg intraperitoneal (i.p.) injection of 50/50% w/v urethane in bacteriostatic 0.9% NaCl (Hospira Inc., Lake Forest, IL). The animals were placed in a stereotaxic frame and holes were drilled through the skull for insertion of the carbon-fiber electrode and Ag/AgCl reference. Three additional holes were drilled 3−5 mm away from the recording location for access to stimulate waves of SD. Coordinates used are in mm anterior-poster (AP), medial-lateral (ML), and dorsal-ventral (DV) with reference to bregma (Paxinos and Watson, 2007). The carbon-fiber working electrode was placed either in the NAc (+2.2 AP, +1.7 ML, −6.9 to −7.4 mm DV) or in the motor cortex (+2.2 AP, +1.7 ML, −0.8 to −2.1 mm DV). The Ag/AgCl electrode was placed in the contralateral hemisphere and secured with a stainless steel screw. The extra holes for stimulations were located at −0.8 AP, +0.8 ML; −0.8 AP, +3.2 ML; and −2.8 AP, +1.7 ML.

Experimental SD. SD-inducing stimuli were delivered at 20 min intervals, 3−5 mm away from the recording site, using either mechanical damage (pinpricks) or delivery of high concentrations of KCl. Hypodermic needles (27 and 22 G) were used to deliver pinpricks to the same depth as the carbon-fiber electrode placement. A 10 μL Hamilton syringe connected to a 33 G infusion needle (Plastics One Inc., Roanoke, VA) was used to manually microinject 2 μL of KCl dissolved in deionized water. Concentrations of 0.25 and 1 M KCl were employed, using the lowest concentration that reliably elicited SD.

Pharmacological investigation of dopamine's effects were performed by i.p. injection of raclopride or SCH 23390 (n = 10 NAc, n = 8 cortex, one drug per location per animal). Two control responses to SD were obtained, followed by 2−4 responses 45 min after drug injection.

Simultaneous Electrochemical and Electrophysiological Data Acquisition. Combined fast-scan cyclic voltammetry (FSCV) and electrophysiological data acquisition has been previously described.[24,55] Briefly, voltage applied to and current recorded at the carbon-fiber microelectrode were managed by the HDCV (High Definition Cyclic Voltammetry, UNC-Chapel Hill, NC, USA) software program. Two different waveforms were used in this study. The "oxygen waveform" simultaneously detects oxygen and dopamine and was used in 16 NAc and 15 cortex locations across 26 rats (in five rats, the electrode was lowered to a second recording location in the same brain region as the first, n = 2 NAc and n = 3 cortex). The waveform was scanned at 400 V/s from 0 to +0.8 V then to −1.4 V before returning to the holding potential of 0 V. A different waveform[24,30] was used to measure dopamine changes and the effects of blocking the dopamine receptors on SD propagation and DC potential changes. The waveform has a 1.5 ms potential step from −0.4 to −0.3 V preceding a triangle scan at 400 V/s from −0.4 to +1.3 V and back to −0.4 V. The potential step serves to determine the impedance of the carbon-fiber microelectrode immediately before each waveform application. In-house software (UNC-Chapel Hill) written in LabVIEW (National Instruments, Austin, TX) performs the subtraction of the convolution-based impedance changes. Single-unit action potentials or DC potential recordings were made in the 180 ms between applications of the voltammetric waveform.

Voltammetric Verification and Calibration. Hobbs et al. describe the verification and calibration techniques employed.[24] An air-impermeable flow-injection analysis system was used to determine the electrodes' (~75 μm exposed carbon fiber) post-experiment sensitivity to oxygen and dopamine. The oxygen waveform has a sensitivity of 1.12 nA/μM for dopamine at its oxidative peak (+0.65 V) and −0.3 nA/μM for oxygen at its reductive peak (−1.33 V). Sensitivity for dopamine on the convolution-based triangle waveform is 7.95 nA/μM.

Data Analysis. Statistical tests were performed in Prism 4 (GraphPad Software, San Diego, CA), and $p < 0.05$ was considered significant. Grubbs' test was used to determine outliers.

Digitizer and Offline Sorter software (Plexon, Dallas, TX) were used to analyze single-unit electrophysiology recordings. DC electrophysiological recordings were analyzed with an in-house MATLAB (Natick, MA) script (Electronics Department, UNC-Chapel Hill).[24]

SD velocity was calculated by dividing the distance between the stimulation and recording sites by the difference in time between the stimulation and onset of the voltammetric SD signal (vertical, gray dashed lines in Figure 1) at the carbon-fiber recording electrode (eq 1).

$$\text{SD velocity} = \frac{\text{distance from stimulation to recording site (mm)}}{\text{time from stimulation to onset of SD signal (min)}} \quad (1)$$

The distances between stimulation and recording sites were obtained from the difference in stereotaxic coordinates. The velocities of successive SDs for a given recording site were averaged, and the means of the NAc and cortex sites were compared by a two-tailed Student's t test. SD velocity over successive waves was assessed by normalizing within-site values to the first SD. The normalized velocities of successive pricks across all recording sites were then grouped and analyzed by ANOVA.

Oxygen traces were analyzed for maxima and minima. Peak magnitude, decay-time ($t_{1/2}$), and half-width analyses for dopamine traces and DC potentials were performed in Clampfit (Molecular Devices, LLC). Within-subject comparisons of these values before and after pharmacological treatment were compared via two-tailed, paired Student's t tests. Averaged values are expressed as mean ± SEM.

AUTHOR INFORMATION

Corresponding Author

*Mailing address: Department of Chemistry and Neuroscience Center, Campus Box 3290, Caudill and Kenan Laboratories, University of North Carolina at Chapel Hill, Chapel Hill, NC 27599, USA. E-mail: rmw@unc.edu. Phone: 919-962-1472.

ORCID

R. Mark Wightman: 0000-0003-2198-139X

Author Contributions

C.N.H. carried out data collection and analysis and wrote the manuscript. G.H. performed surgeries, collected and analyzed data, and made electrodes. A.S.M. performed surgeries and collected data. C.N.H. and R.M.W. designed the experiments. All authors read and approved the final version of this manuscript.

DOI: 10.1021/acschemneuro.7b00266
ACS Chem. Neurosci. 2017, 8, 2512−2521

Funding
This research was supported by a grant from the NIH (DA032530 to R.M.W.).

Notes
The authors declare no competing financial interest.

■ ACKNOWLEDGMENTS
Daniel Seebold performed surgeries and made electrodes.

■ ABBREVIATIONS
SD, spreading depolarization; FSCV, fast-scan cyclic voltammetry; NAc, nucleus accumbens; i.p., intraperitoneal

■ REFERENCES
(1) Dreier, J. P., Isele, T., Reiffurth, C., Offenhauser, N., Kirov, S. A., Dahlem, M. A., and Herreras, O. (2013) Is spreading depolarization characterized by an abrupt, massive release of gibbs free energy from the human brain cortex? *Neuroscientist 19*, 25−42.
(2) Somjen, G. G. (2001) Mechanisms of spreading depression and hypoxic spreading depression-like depolarization. *Physiol Rev. 81*, 1065−1096.
(3) Hansen, A. J., and Zeuthen, T. (1981) Extracellular ion concentrations during spreading depression and ischemia in the rat brain cortex. *Acta Physiol. Scand. 113*, 437−445.
(4) Kraio, R. P., and Nicholson, C. (1978) Extracellular ionic variations during spreading depression. *Neuroscience 3*, 1045−1059.
(5) Fabricius, M., Jensen, L. H., and Lauritzen, M. (1993) Microdialysis of interstitial amino acids during spreading depression and anoxic depolarization in rat neocortex. *Brain Res. 612*, 61−69.
(6) Szerb, J. C. (1991) Glutamate release and spreading depression in the fascia dentata in response to microdialysis with high K+: role of glia. *Brain Res. 542*, 259−265.
(7) Moghaddam, B., Schenk, J. O., Stewart, W. B., and Hansen, A. J. (1987) Temporal Relationship between Neurotransmitter Release and Ion Flux during Spreading Depression and Anoxia. *Can. J. Physiol. Pharmacol. 65*, 1105−1110.
(8) Kaku, T., Hada, J., and Hayashi, Y. (1994) Endogenous adenosine exerts inhibitory effects upon the development of spreading depression and glutamate release induced by microdialysis with high K+ in rat hippocampus. *Brain Res. 658*, 39−48.
(9) Ngo, K. T., Varner, E. L., Michael, A. C., and Weber, S. G. (2017) Monitoring Dopamine Responses to Potassium Ion and Nomifensine by in Vivo Microdialysis with Online Liquid Chromatography at One-Minute Resolution. *ACS Chem. Neurosci. 8*, 329−338.
(10) Ayata, C., and Lauritzen, M. (2015) Spreading Depression, Spreading Depolarizations, and the Cerebral Vasculature. *Physiol. Rev. 95*, 953−993.
(11) Sonn, J., and Mayevsky, A. (2000) Effects of brain oxygenation on metabolic, hemodynamic, ionic and electrical responses to spreading depression in the rat. *Brain Res. 882*, 212−216.
(12) Back, T., Kohno, K., and Hossmann, K. A. (1994) Cortical negative DC deflections following middle cerebral artery occlusion and KCl-induced spreading depression: effect on blood flow, tissue oxygenation, and electroencephalogram. *J. Cereb. Blood Flow Metab. 14*, 12−19.
(13) Mies, G., and Paschen, W. (1984) Regional changes of blood flow, glucose, and ATP content determined on brain sections during a single passage of spreading depression in rat brain cortex. *Exp. Neurol. 84*, 249−258.
(14) Shin, H. K., Dunn, A. K., Jones, P. B., Boas, D. A., Moskowitz, M. A., and Ayata, C. (2006) Vasoconstrictive neurovascular coupling during focal ischemic depolarizations. *J. Cereb. Blood Flow Metab. 26*, 1018−1030.
(15) Dreier, J. P., Major, S., Manning, A., Woitzik, J., Drenckhahn, C., Steinbrink, J., Tolias, C., Oliveira-Ferreira, A. I., Fabricius, M., Hartings, J. A., Vajkoczy, P., Lauritzen, M., Dirnagl, U., Bohner, G., and Strong, A. J. (2009) Cortical spreading ischaemia is a novel process involved in ischaemic damage in patients with aneurysmal subarachnoid haemorrhage. *Brain 132*, 1866−1881.
(16) Mies, G., Iijima, T., and Hossmann, K.-A. (1993) Correlation between periinfarct DC shifts and ischaemic neuronal damage in rat. *NeuroReport 4*, 709−711.
(17) Dijkhuizen, R. M., Beekwilder, J. P., van der Worp, H. B., van der Sprenkel, J. W. B., Tulleken, K. A. F., and Nicolay, K. (1999) Correlation between tissue depolarizations and damage in focal ischemic rat brain. *Brain Res. 840*, 194−205.
(18) Hartings, J. A., Rolli, M. L., Lu, X. C., and Tortella, F. C. (2003) Delayed secondary phase of peri-infarct depolarizations after focal cerebral ischemia: relation to infarct growth and neuroprotection. *J. Neurosci. 23*, 11602−11610.
(19) Dietrich, W. D., Feng, Z.-C., Leistra, H., Watson, B. D., and Rosenthal, M. (1994) Photothrombotic infarction triggers multiple episodes of cortical spreading depression in distant brain regions. *J. Cereb. Blood Flow Metab. 14*, 20−28.
(20) Piilgaard, H., and Lauritzen, M. (2009) Persistent increase in oxygen consumption and impaired neurovascular coupling after spreading depression in rat neocortex. *J. Cereb. Blood Flow Metab. 29*, 1517−1527.
(21) Sakadžić, S., Yuan, S., Dilekoz, E., Ruvinskaya, S., Vinogradov, S. A., Ayata, C., and Boas, D. A. (2009) Simultaneous imaging of cerebral partial pressure of oxygen and blood flow during functional activation and cortical spreading depression. *Appl. Opt. 48*, D169−D177.
(22) Balanca, B., Meiller, A., Bezin, L., Dreier, J. P., Marinesco, S., and Lieutaud, T. (2017) Altered hypermetabolic response to cortical spreading depolarizations after traumatic brain injury in rats. *J. Cereb. Blood Flow Metab. 37*, 1670−1686.
(23) Takano, T., Tian, G. F., Peng, W., Lou, N., Lovatt, D., Hansen, A. J., Kasischke, K. A., and Nedergaard, M. (2007) Cortical spreading depression causes and coincides with tissue hypoxia. *Nat. Neurosci. 10*, 754−762.
(24) Hobbs, C. N., Johnson, J. A., Verber, M. D., and Wightman, R. M. (2017) An Implantable Multimodal Sensor for Oxygen, Neurotransmitters, and Electrophysiology during Spreading Depolarization in the Deep Brain. *Analyst 142*, 2912−2920.
(25) Bureš, J., and Burešová, O. (1981) Cerebral [K+] e increase as an index of the differential susceptibility of brain structures to terminal anoxia and electroconvulsive shock. *J. Neurobiol. 12*, 211−220.
(26) Cavaglia, M., Dombrowski, S. M., Drazba, J., Vasanji, A., Bokesch, P. M., and Janigro, D. (2001) Regional variation in brain capillary density and vascular response to ischemia. *Brain Res. 910*, 81−93.
(27) Surmeier, D. J., Ding, J., Day, M., Wang, Z., and Shen, W. (2007) D1 and D2 dopamine-receptor modulation of striatal glutamatergic signaling in striatal medium spiny neurons. *Trends Neurosci. 30*, 228−235.
(28) Pockberger, H. (1991) Electrophysiological and morphological properties of rat motor cortex neurons in vivo. *Brain Res. 539*, 181−190.
(29) Li, C., Narayan, R. K., Wang, P., and Hartings, J. A. (2017) Regional temperature and quantitative cerebral blood flow responses to cortical spreading depolarization in the rat. *J. Cereb. Blood Flow Metab. 37*, 1634−1640.
(30) Johnson, J. A., Hobbs, C. N., and Wightman, R. M. (2017) Removal of Differential Capacitive Interferences in Fast-Scan Cyclic Voltammetry. *Anal. Chem. 89*, 6166−6174.
(31) Ayata, C. (2013) Pearls and pitfalls in experimental models of spreading depression. *Cephalalgia 33*, 604−613.
(32) Karunasinghe, R. N., and Lipski, J. (2013) Oxygen and glucose deprivation (OGD)-induced spreading depression in the Substantia Nigra. *Brain Res. 1527*, 209−221.
(33) Brisson, C. D., and Andrew, R. D. (2012) A neuronal population in hypothalamus that dramatically resists acute ischemic injury compared to neocortex. *J. Neurophysiol. 108*, 419−430.
(34) Lian, X. Y., and Stringer, J. L. (2004) Energy failure in astrocytes increases the vulnerability of neurons to spreading depression. *Eur. J. Neurosci 19*, 2446−2454.
(35) Fujita, S., Mizoguchi, N., Aoki, R., Cui, Y., Koshikawa, N., and Kobayashi, M. (2016) Cytoarchitecture-dependent decrease in

DOI: 10.1021/acschemneuro.7b00266
ACS Chem. Neurosci. 2017, 8, 2512−2521

propagation velocity of cortical spreading depression in the rat insular cortex revealed by optical imaging. *Cereb Cortex 26*, 1580−1589.
(36) Savchenko, V., McKanna, J., Nikonenko, I., and Skibo, G. (2000) Microglia and astrocytes in the adult rat brain: comparative immunocytochemical analysis demonstrates the efficacy of lipocortin 1 immunoreactivity. *Neuroscience 96*, 195−203.
(37) Duckrow, R. B. (1991) Regional cerebral blood flow during spreading cortical depression in conscious rats. *J. Cereb. Blood Flow Metab. 11*, 150−154.
(38) Rogers, M. L., Feuerstein, D., Leong, C. L., Takagaki, M., Niu, X., Graf, R., and Boutelle, M. G. (2013) Continuous online microdialysis using microfluidic sensors: dynamic neurometabolic changes during spreading depolarization. *ACS Chem. Neurosci. 4*, 799−807.
(39) Chang, J. C., Shook, L. L., Biag, J., Nguyen, E. N., Toga, A. W., Charles, A. C., and Brennan, K. C. (2010) Biphasic direct current shift, haemoglobin desaturation and neurovascular uncoupling in cortical spreading depression. *Brain 133*, 996−1012.
(40) Verhaegen, M. J., Todd, M. M., Warner, D. S., James, B., and Weeks, J. B. (1992) The role of electrode size on the incidence of spreading depression and on cortical cerebral blood flow as measured by H2 clearance. *J. Cereb. Blood Flow Metab. 12*, 230−237.
(41) Wolf, T., Lindauer, U., Villringer, A., and Dirnagl, U. (1997) Excessive oxygen or glucose supply does not alter the blood flow response to somatosensory stimulation or spreading depression in rats. *Brain Res. 761*, 290−299.
(42) Zimmerman, J. B., and Wightman, R. M. (1991) Simultaneous electrochemical measurements of oxygen and dopamine in vivo. *Anal. Chem. 63*, 24−28.
(43) Brennan, K. C., Beltran-Parrazal, L., López-Valdés, H. E., Theriot, J., Toga, A. W., and Charles, A. C. (2007) Distinct vascular conduction with cortical spreading depression. *J. Neurophysiol. 97*, 4143−4151.
(44) Fabricius, M., Akgoren, N., and Lauritzen, M. (1995) Arginine-nitric oxide pathway and cerebrovascular regulation in cortical spreading depression. *Am. J. Physiol. 269*, H23−H29.
(45) Boero, J. A., Ascher, J., Arregui, A., Rovainen, C., and Woolsey, T. A. (1999) Increased brain capillaries in chronic hypoxia. *J. Appl. Physiol. 86*, 1211−1219.
(46) Klein, B., Kuschinsky, W., Schrock, H., and Vetterlein, F. (1986) Interdependency of local capillary density, blood flow, and metabolism in rat brains. *Am. J. Physiol. 251*, H1333−H1340.
(47) Ayata, C., Shimizu-Sasamata, M., Lo, E., Noebels, J., and Moskowitz, M. (1999) Impaired neurotransmitter release and elevated threshold for cortical spreading depression in mice with mutations in the α1A subunit of P/Q type calcium channels. *Neuroscience 95*, 639−645.
(48) Marrannes, R., Willems, R., Deprins, E., and Wauquier, A. (1988) Evidence for a Role of the N-Methyl-D-Aspartate (NMDA) Receptor in Cortical Spreading Depression in the Rat. *Brain Res. 457*, 226−240.
(49) van Harreveld, A. (1959) Compounds in brain extracts causing spreading depression of cerebral cortical activity and contraction of crustacean muscle. *J. Neurochem. 3*, 300−315.
(50) Grafstein, B. (1956) Mechanism of spreading cortical depression. *J. Neurophysiol. 19*, 154−171.
(51) Belle, A. M., Owesson-White, C., Herr, N. R., Carelli, R. M., and Wightman, R. M. (2013) Controlled iontophoresis coupled with fast-scan cyclic voltammetry/electrophysiology in awake, freely moving animals. *ACS Chem. Neurosci. 4*, 761−771.
(52) Missale, C., Nash, S. R., Robinson, S. W., Jaber, M., and Caron, M. G. (1998) Dopamine receptors: from structure to function. *Physiol Rev. 78*, 189−225.
(53) Nagy, G., Moghaddam, B., Oke, A., and Adams, R. N. (1985) Simultaneous monitoring of voltammetric and ion-selective electrodes in mammalian brain. *Neurosci. Lett. 55*, 119−124.
(54) Nicola, S. M., Surmeier, D. J., and Malenka, R. C. (2000) Dopaminergic modulation of neuronal excitability in the striatum and nucleus accumbens. *Annu. Rev. Neurosci. 23*, 185−215.
(55) Takmakov, P., McKinney, C. J., Carelli, R. M., and Wightman, R. M. (2011) Instrumentation for fast-scan cyclic voltammetry combined with electrophysiology for behavioral experiments in freely moving animals. *Rev. Sci. Instrum. 82*, 074302.

DOI: 10.1021/acschemneuro.7b00266
ACS Chem. Neurosci. 2017, 8, 2512−2521